Precipitation and its influence on the phase transition in Cu-14.1 wt.% Al-4.2 wt.% Ni shape memory alloy

1993 J. Phys.: Condens. Matter 5 2719

(http://iopscience.iop.org/0953-8984/5/17/006)

J. Phys.: Condens. Matter 5 (1993) 2719–2728. Printed in the UK

Precipitation and its influence on the phase transition in Cu–14.1 wt% Al–4.2 wt% Ni shape memory alloy

Yimin Zhang†‡§, Jianian Gui†‡, Renhui Wang†‡, Lamei Gao†, Yigui Wu§ and Yali Tang||

† Department of Physics, Wuhan University, 430072 Wuhan, People's Republic of China
‡ Beijing Laboratory of Electron Microscopy, Chinese Academy of Sciences, 100080 Beijing, People's Republic of China
§ Luoyang Institute of Technology, 471039 Luoyang, People's Republic of China
|| Zhengzhou Institute of Technology, 450002 Zhengzhou, People's Republic of China

Received 5 January 1993

Abstract. The precipitation behaviour of a Cu–14.1 wt% Al–4.2 wt% Ni shape memory alloy and its effect on the phase constituents, fine structure and thermoelastic martensitic transformation have been studied using x-ray diffraction analysis, transmission electron microscopy and acoustic emission techniques. In the 700 K step-quenched specimens, a γ_2-phase with a complex cubic structure precipitates coherently from the parent phase. The γ_2 precipitate is rich in alloying elements which causes the retained parent phase to be poor in the alloying elements and hence increases the martensite transition temperature of the step-quenched specimens. The coherent strain field may influence the structure types and the fine structures of the transformed martensite. Finally, the cooling rate of the retained parent phase during quenching influences the domain size of the parent phase and the martensites transformed from the parent phase.

1. Introduction

Compared with Ti–Ni shape memory alloys (SMAs) which are the mostly popular SMAs on the market, Cu-based SMAs have the advantage of a lower price. Among Cu-based SMAs, Cu–Al–Ni alloys show a better thermal stability than Cu–Zn–Al alloys do. Sakamoto and Shimizu [1] reviewed recently some problems in developing Cu–Al–Ni SMAs, one of which is the variation in characteristics of the martensitic transformation with heat treatment. Along this line, Sakamoto and Shimizu [2] and Gui *et al* [3] studied the effects of composition and heat treatment on the phase constituents, the size of the ordered domains and the martensitic transformation characteristics of some Cu–Al–Ni SMAs.

As reviewed by Miyazaki and Otsuka [4], the composition of the practically applicable Cu–Al–Ni SMA lies near Cu–14 wt% Al–4 wt% Ni, corresponding to the Cu_3Al binary alloy. Such alloys exist as a single β-phase at high temperatures with A2-type disordered, B2-type (CsCl-type) ordered, $D0_3$-type (Fe_3Al-type) or $L2_1$-type (Cu_2MnAl Heusler alloy) ordered structures, depending on the composition and temperature (see the review by Shimizu and Tadaki [5] and the book by Barrett and Massalski [6]). The Cu–12 wt% Al alloy will transform eutectoidally into the face-centred cubic α-phase and the γ_2-phase of the γ-brass structure [6] when slowly cooled through the eutectoid temperature (838 K). Rapid quenching may inhibit the eutectoid reaction and promote the martensitic transformation

0953-8984/93/172719+10$07.50

at the temperature M_s. 9R-, 18R-, 2H- and/or 6R-type martensites [5] may be formed depending on the composition, ordering, stress state and other fine structures of the parent phase. The purpose of adding Ni to the Cu–Al alloy is to depress the diffusivity of Cu or Al, hence inhibiting the precipitation of the γ_2-phase and promoting the thermoelastic martensitic transformation. According to Miyazaki and Otsuka [4], M_s for the Cu–Al–Ni SMA will decrease by about 13 °C when the Al content is increased by 0.1 wt%. Therefore, control of the phase transformation temperature is another important problem in developing Cu–Al–Ni SMAs.

In the present work we study the precipitation behaviour and its influence on the characteristics of the martensitic transformation of Cu–14.1 wt% Al–4.2 wt% Ni SMA when the alloy is subjected to different heat treatments. Such a study will help understanding of the mechanism of the shape memory effect in the Cu–Al–Ni SMA and development of this type of SMA.

2. Specimen preparation and experimental method

Cu–14.1 wt% Al–4.2 wt% Ni alloy was hot rolled to plate specimens 1.5 mm in thickness and then heat treated by four different procedures as listed in table 1.

Table 1. Heat treatments of the Cu–14.1 wt% Al–4.2 wt% Ni specimens.

Specimen	Heat treatment
Directly quenched	Solid solution heated at 1223 K for 5 min; then quenched into cold 10% NaOH solution
One step quenched	1223 K for 5 min → 700 K salt bath for 40 s → cold 10% NaOH solution
Two step quenched	1223 K for 5 min → 700 K salt bath for 40 s → 373 K water or 430 K oil for 4 min → air cooled

All the heat-treated plate specimens were studied first by using an XD-3A x-ray diffractometer with Cu Kα radiation. Their martensite transition temperatures A_s and M_s were measured using the acoustic emission technique.

Foils for transmission electron microscopy (TEM) were prepared from the plate specimens first by chemical thinning in a solution of $HCl:HNO_3:H_3PO_4 = 1:4:5$ and then by twin-jet electropolishing in a solution of $HNO_3:CH_3OH = 1:2$ at room temperature. TEM observation was carried out using a Philips EM-420 microscope equipped with a double-tilting goniometer and operated at 100 kV. Systematic tilt experiments were carried out in order to obtain a series of electron diffraction patterns (EDPs) to identify the structure of the martensites and precipitates. In order to reveal the B2-type and $D0_3$-type order domain boundaries, centred dark-field (DF) images were photographed under the two-beam condition using the following superlattice reflections: for the parent β_1-phase, (222) and (111) diffraction spots near the $[0\bar{1}1]_{\beta_1}$ zone axis were used to display the B2-type and $D0_3$-type domain boundaries, respectively; for 2H martensite, (223) (for B2-type ordering) and (112) (for $D0_3$-type ordering) reflections near the $[1\bar{1}0]_{2H}$ zone axis were used.

3. Experimental results

So far as the experimental methods used in this study show, there is no discernible difference between the 700 K → 373 K and 700 K → 430 K two-step-quenched specimens.

3.1. X-ray diffraction analysis

Figure 1 shows a part of the room-temperature polycrystalline x-ray diffraction patterns ($2\theta = 25°–50°$), in which the relevant phases and indices for each peak are marked. From the x-ray diffraction analysis we find that the directly quenched specimen consists of $D0_3$ order parent β_1-phase, the one-step-quenched specimen consists mainly of $18R_1$ (major phase) and 2H martensites, and the two-step-quenched specimens consist mainly of 2H martensite.

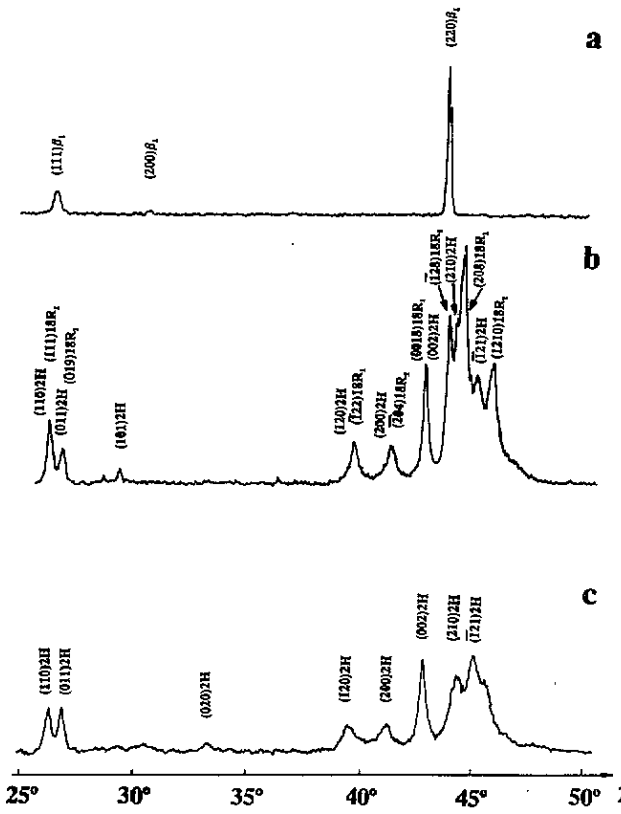

Figure 1. Polycrystalline x-ray diffraction patterns of the Cu–14.1 wt% Al–4.2 wt% Ni specimens: (*a*) directly quenched specimen; (*b*) one-step-quenched specimen; (*c*) 373 K two-step-quenched specimen.

The apparent characteristic of the x-ray diffraction patterns from step-quenched specimens is the broad peaks. For example, the full widths $\Delta(2\theta)$ at half-maximum of the $(002)_{2H}$ and $(320)_{2H}$ peaks are 0.4° and 0.8°, respectively, for the step-quenched specimens compared with $\Delta(2\theta) = 0.20°$ for the $(220)_{\beta_1}$ or $(400)_{\beta_1}$ peak of the directly quenched specimens.

3.2. Electron diffraction and energy-dispersive x-ray spectroscopy analysis

Electron diffraction experiments show that the directly quenched specimen consists only of DO_3 order parent β_1-phase. In the one-step-quenched specimen both $18R_1$-type and 2H-type martensites were identified. Figure 2 shows a series of EDPs and their indexing of the 2H-type martensite which inherited the DO_3 ordering of the parent β_1-phase. The EDPs of $18R_1$-type martensite observed in the present work are similar to those already published in [7]. In both the two-step-quenched specimens the only martensite identified is the 2H type. Moreover, there are cubic γ_2 precipitates of γ-brass structure dispersively distributed in the one-step-quenched (figure 3(*b*)) and two-step-quenched (figure 3(*a*)) specimens. These γ_2 precipitates have a lattice constant of 0.87 nm and particle sizes of about 50 nm (dispersively distributed) and 0.2–1.0 μm (isolated). Figure 4 shows a series of EDPs and their indexing of the γ_2-phase. This selected-area electron diffraction (SAED) experiment shows that these step-quenched specimens contain the γ_2-phase in addition to martensite.

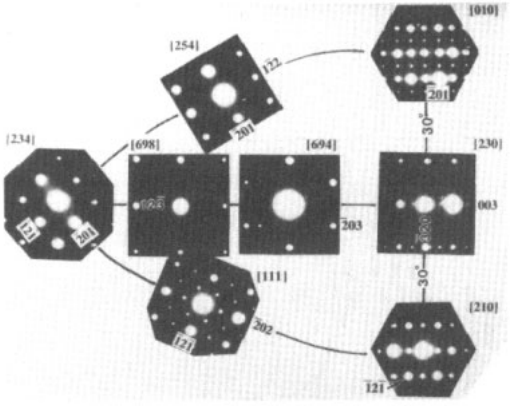

Figure 2. EDPs of the 2H-type martensite.

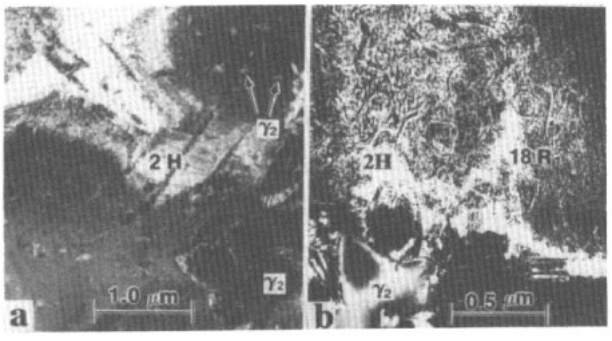

Figure 3. DF images of the Cu–14.1 wt% Al–4.2 wt% Ni alloy: (*a*) 373 K two-step-quenched specimen, $\boldsymbol{g} = (223)_{2H}$, showing dispersively distributed γ_2 precipitates; (*b*) one-step-quenched specimen, $\boldsymbol{g} = (002)_{2H} = (0\,0\,18)_{18R_1}$.

The compositions of all the phases in differently heat-treated specimens were analysed using an energy-dispersive x-ray spectrometer in conjunction with a JEOL JEM 2000FX transmission electron microscope. Table 2 lists the main results of the energy-dispersive

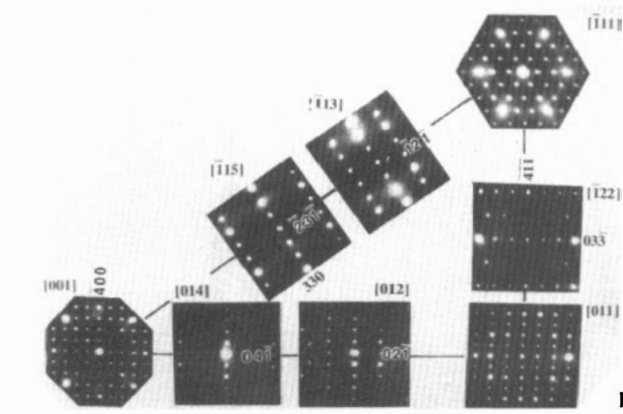

Figure 4. EDPs of the γ_2-phase.

spectroscopy (EDS) analysis which reveals that the γ_2-phase is rich in the alloying elements Al and Ni, and the 2H martensite contains a smaller amount of alloying elements than does the average composition, i.e. the composition of the β_1-phase which is the only constituent phase of the directly quenched specimen. The difference between the EDS measured average composition (Cu–12.5 wt% Al–4.1 wt% Ni) and the nominal composition (Cu–14.1 wt% Al–4.2 wt% Ni) arises because of the uncertainty in the EDS quantitative analysis, but this uncertainty does not affect the conclusion about the relative relationship of the enrichment of the alloying elements.

Table 2. Compositions of the constituent phases in differently heat-treated Cu–14.1 wt% Al–4.2 wt% Ni specimens.

		Composition (wt%)		
Specimen	Phase	Cu	Al	Ni
Directly quenched	β_1	83.4	12.5	4.1
700 K → 430 K two step quenched	2H	84.3	11.9	3.8
700 K → 430 K two step quenched	γ_2	76.0	18.2	5.8

3.3. Phase transition behaviour

The variation in the acoustic emission ringdown count rate $\dot{N}$ with temperature of the differently heat-treated specimens reveals that all these specimens show thermoelastic martensitic transformations and that the transition temperatures of the step-quenched specimens are higher than those of the directly quenched specimen by about 94 K. Moreover, one-step-quenched specimens show a two-stage reverse martensitic transformation with $A_{s1} = 318$ K and $A_{s2} = 330$ K. Figures 5(*a*) and 5(*b*) show the acoustic emission curves of one-step-quenched and two-step-quenched specimens, respectively.

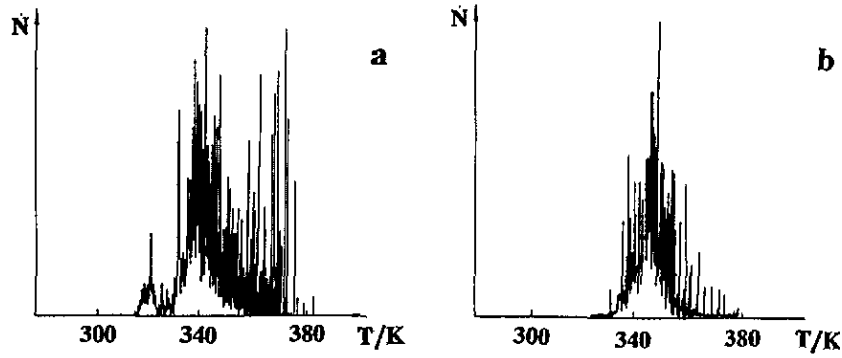

Figure 5. Acoustic emission curves showing the variation in the ringdown count rate $\dot{N}$ with temperature of the Cu–14.1 wt% Al–4.2 wt% Ni specimens during heating: (*a*) one-step-quenched specimen; (*b*) 430 K two-step-quenched specimen.

3.4. TEM study of the γ_2 precipitates

All the step-quenched specimens contain γ_2 precipitates as shown in figure 6(*a*) which is a DF image of the one-step-quenched specimen when the $(220)_{\gamma_2}$ reflection is excited. In this picture, γ_2 precipitates coexist with the 2H martensite. In the image the phase boundaries are blurred. Figure 6(*b*) shows the EDP of the 2H martensite along its $[0\bar{1}0]_{2H}$ zone axis. Figures 6(*c*) and 6(*d*) are SAED and convergent-beam electron diffraction (CBED) patterns, respectively, of the γ_2 precipitate when its neighbour 2H martensite is oriented exactly along the $[0\bar{1}0]_{2H}$ zone axis. Figure 6(*c*) shows that this γ_2-phase is nearly along the $[001]_{\gamma_2}$ zone axis. In figure 6(*d*) the $[001]_{\gamma_2}$ zone axis is indicated by a white star and the incident beam by a letter *O*. This CBED pattern shows that the γ_2-phase deviates by *1.0°* from its $[001]_{\gamma_2}$ direction in its (100) plane when its neighbouring 2H martensite lies along the $[0\bar{1}0]_{2H}$ direction. From this and from the lattice constants of the γ_2-phase and the 2H phase [8] we obtain the lattice correspondence between the γ_2 precipitate and the 2H martensite as follows:

$$\begin{aligned}&(10\bar{1})_{2H} \sim (300)_{\gamma_2}\\ &\tfrac{1}{2}[0\bar{1}0]_{2H} \sim \tfrac{1}{3}[001]_{\gamma_2}.\end{aligned} \tag{1}$$

A clear CBED pattern such as figure 6(*d*) can be obtained only when the incident electron probe lies in the middle of the γ_2-phase. When the incident probe lies near the γ_2–2H boundary, the CBED pattern becomes blurred and distorted. The blurring of both the contrast image and the CBED pattern at the γ_2–2H phase boundary shows that a strong strain field exists.

3.5. Order domains and stacking faults

Figure 7 shows a set of DF images under the two-beam condition when different superlattice reflections are excited. Such DF images reveal that the size of the B2 domains (figure 7(*b*)) is much larger than the DO_3 domains (figure 7(*a*)) in the directly quenched specimens. The one-step- and two-step-quenched specimens contain a high density of stacking faults which appear as vertical stripes in figures 7(*c*) and 7(*d*). These stripes have disturbed the observation of the domain structure in the step-quenched specimens. Close observation

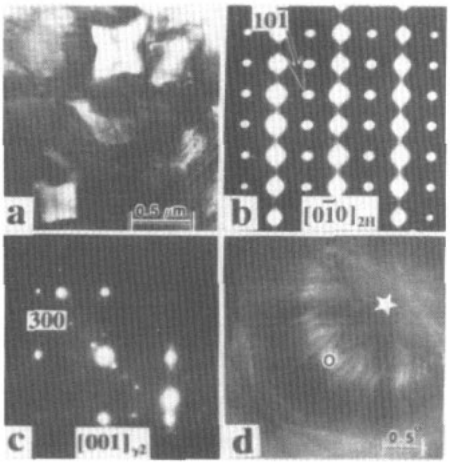

Figure 6. Precipitates in the one-step-quenched Cu–14.1 wt% Al–4.2 wt% Ni specimen: (*a*) $(220)_{\gamma_2}$ DF image; (*b*) EDP of 2H martensite along the $[0\bar{1}0]_{2H}$ zone axis; (*c*) EDP of the γ_2-phase near the $[001]_{\gamma_2}$ zone axis; (*d*) CBED pattern near the $[001]_{\gamma_2}$ zone axis.

reveals that the size of the B2-type domains is still larger than that of the $D0_3$-type domains in the step-quenched specimens, and both the B2 and the $D0_3$ domains of the step-quenched specimens, respectively, are larger than those of the directly quenched specimens. Moreover, there is no discernible difference between the differently step-quenched specimens observed by TEM DF imaging.

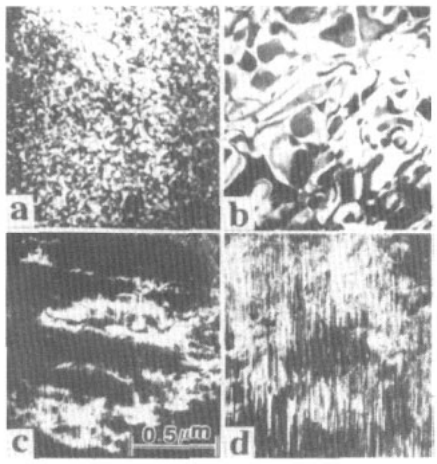

Figure 7. DF images of the Cu–14.1 wt% Al–4.2 wt% Ni specimens showing the B2- or $D0_3$-type order domain structure and stacking faults: (*a*) directly quenched specimen, $\boldsymbol{g} = (111)_{\beta_1}$, $D0_3$-type domains; (*b*) directly quenched specimen, $\boldsymbol{g} = (222)_{\beta_1}$, B2-type domains; (*c*) one-step-quenched specimen, $\boldsymbol{g} = (112)_{2H}$, $D0_3$-type domains; (*d*) one-step-quenched specimen, $\boldsymbol{g} = (223)_{2H}$ B2-type domains.

Figure 3(*b*) shows another DF image of the one-step-quenched specimen when $(002)_{2H} = (00\,18)_{18R_1}$ reflections are excited. In this picture the γ_2 precipitate and the 2H and $18R_1$ martensites coexist as revealed by SAED experiments. There is no distinct boundary between the 2H and $18R_1$ martensites and the contrast of the order domain boundaries crosses this boundary continuously.

Some characteristics of the Cu–14.1 wt% Al–4.2 wt% Ni alloy after different heat treatments are summarized in table 3.

Table 3. Summary of the characteristics of the Cu–14.1 wt% Al–4.2 wt% Ni alloy after different heat treatments.

Specimen	Phase constituents	A_s (K)	M_s (K)	B_2 domain size (nm)	$D0_3$ domain size (nm)	Stacking faults	X-ray diffraction peak width $\Delta(2\theta)$ (deg)
Directly quenched	β_1	—	240	200	50	No	0.2 (narrow)
One step quenched	$18R_1$(major)+2H + γ_2(minor)	318 (A_{s_1}), 330 (A_{s_2})	334	500	250	Dense	0.4–0.8 (broad)
Two step quenched	2H(major)+γ_2(minor)	332	334	500	250	Dense	0.4–0.8 (broad)

4. Discussion

Our experiments reveal that step quenching at 700 K causes the precipitation of a complex cubic phase which is rich in the alloying elements Al and Ni. This decreases in turn the content of the alloying elements in the retained parent phase. From the temperatures M_s listed in [4] we conclude that M_s will increase by about 130 K and 70 K when the Al and Ni contents, respectively, of the parent phase are decreased by 1.0 wt%. According to the EDS measured data listed in table 2 of the present paper, the retained parent phase in the step-quenched specimen possesses less Al (by 0.6 wt%) and Ni (by 0.3 wt%) than does the directly quenched specimen. This decrease would cause M_s to increase by about 99 K which is in good agreement with the measured M_s-values listed in table 3, which shows a 94 K increase in M_s for the step-quenched specimens compared with the directly quenched specimens. This effect may be used to adjust the transition temperature of the SMAs.

Shimizu and Tadaki [5] and Sakamoto and Shimizu [1] summarized the stress–temperature phase diagram for Cu–Al–Ni alloys. According to this phase diagram, the transformed martensite is $18R_1$ type when an intermediate stress exists. For the one-step-quenched specimen the cooling rate (and hence the thermal stress) is larger than for the two-step-quenched specimens. This may promote the formation of $18R_1$ martensite in the one-step-quenched specimens. In addition, Sakamoto and Shimizu [1] interpreted similar effects by different orderings of the differently heat-treated specimens.

It is well known [5] that both the 2H and the $18R_1$ martensites possess the following lattice correspondences:

$$\begin{aligned} &[0\bar{1}0]_{M} \sim [001]_{\beta_1} \\ &(0\,0\,18)_{18R_1} \sim (002)_{2H} \sim (220)_{\beta_1} \end{aligned} \tag{2}$$

which means that the 2H and $18R_1$ martensites possess the same base plane and their difference lies only in different stacking modes parallel to the base planes. This explains the indistinguishable boundary between these two types of martensite.

From the lattice correspondence (2), one obtains

$$(10\bar{1})_{2H} \sim (200)_{\beta_1}. \tag{3}$$

On combination of the observed lattice correspondence (1) between the γ_2-phase and the 2H martensite and the lattice correspondences (2) and (3) between the 2H martensite and the parent β_1-phase it is easy to deduce the lattice correspondence between the γ_2 precipitate and the parent phase as follows:

$$\begin{aligned} &(300)_{\gamma_2} \sim (200)_{\beta_1} \\ &\tfrac{1}{3}[001]_{\gamma_2} \sim \tfrac{1}{2}[001]_{\beta_1}. \end{aligned} \tag{4}$$

This relationship is quite simple to understand by noting [6] that the parent β_1-phase is an ordered structure of the body-centred cubic (BCC) A2-type structure and the unit cell of the β_1-phase consists of eight BCC unit cells. On the other hand, the unit cell of the γ-brass may be described as consisting of 27 BCC unit cells with some minor adjustment of the atoms. From this, one can deduce that the γ_2-phase precipitates coherently from the parent phase and hence causes a coherent strain field.

In conventional Cu–Al–Ni SMAs the fine structure of the 2H martensite consists mainly of microtwins. In the present work we found both twins and densely distributed stacking

faults in the 2H martensites in step-quenched Cu–Al–Ni specimens. The strong strain field near the γ_2 precipitates may be the reason for the dense stacking faults in 2H martensite transformed from the parent phase with uneven strain fields. The 2H martensite with such dense stacking faults still shows good reverse martensitic transformation behaviour. Therefore, the existence of stacking faults is not the reason for the poor thermoelasticity.

The domain size difference for differently heat-treated specimens may be explained as follows: the cooling rate during direct quenching is larger and hence the supercooling for the A2 $\rightarrow$ B2 $\rightarrow$ DO_3, transition of the parent phase is also larger than those during step quenching. Therefore, there are more nuclei in the order domains of the parent phase of the directly quenched specimens, which results in the smaller domains. This quenching rate effect is the same as that for Cu–Zn–Al SMAs [7].

Acknowledgment

This project was supported by the National Natural Science Foundation of China.

References

[1] Sakamoto H and Shimizu K 1989 *Mem. Inst. Sci. Indust. Res. Osaka Univ.* **46** 99
[2] Sakamoto H and Shimizu K 1989 *Iron Steel Inst. Japan Int.* **29** 395
[3] Gui J, Ren Q and Wang R 1991 *Acta Met. Sin. (Engl. Edn)* A **4** 446
[4] Miyazaki S and Otsuka K 1984 *Shape Memory Alloys* ed H Funakubo (Tokyo: Industry Books) p 94 (in Japanese)
[5] Shimizu K and Tadaki T 1984 *Shape Memory Alloys* ed H Funakubo (Tokyo: Industry Books) p 1 (in Japanese)
[6] Barrett C S and Massalski T B 1966 *Structure of Metals* (New York: McGraw-Hill) p 27
[7] Gui J, Luo C, Zhang H, Hu W and Wang R 1990 *J. Mater. Sci.* **25** 1675
[8] Agafonov V, Naudot P, Dubertret A and Dubois B 1988 *Scr. Metall.* **22** 489